



Empowering Minimally Invasive Bioelectronic Devices: Silver-Enhanced Magnetolectric Wireless Power Transfer For Unprecedented Power Density And Advanced Capabilities

Layla Ali jaffar*

*Department Clinical Laboratory Science / College of Pharmacy/Mustansiriyah University. laylaali89m@uomustansiriyah.edu.iq

Citation: Layla Ali jaffar, et al. (2024), Empowering Minimally Invasive Bioelectronic Devices: Silver-Enhanced Magnetolectric Wireless Power Transfer For Unprecedented Power Density And Advanced Capabilities, *Educational Administration: Theory and Practice*, 30(3), 535-544, Doi: 10.53555/kuey.v30i3.1309

ARTICLE INFO

ABSTRACT

Introduction: “Wireless Power Transfer (WPT)” helps miniaturize and extend the lifetime of “implanted medical devices (IMDs)”. Traditional magnetic field inductive coupling is common. Health-conscious and ageing populations are driving wearable and implanted electronics, which enable biological signal monitoring. Advanced flexible bio-integrated circuits, MEMS, and biocompatible materials improve signal accuracy and patient comfort. Developing minimally invasive, lightweight power sources with flexibility and biocompatibility for next-gen bioelectronics remains difficult.

Aim and objectives: The study aims to improve the power density and capabilities of minimally invasive bioelectronic devices by using silver-enhanced magnetolectric wireless power transmission.

Method: The “Wireless Power Transfer System (WPTS)” uses an Equivalent Circuit Model to transform magnetic waves to mechanical vibrations and piezoelectrically to electrical energy, unlike the RIC design. The ME transducer, having a PZT layer between Galfenol layers, receives and a circular coil transmits. Interface coupling coefficients affect ME coupling. Experimental validation uses a single-coil RF power amplifier to create a magnetic field and test the transducer’s performance.

Result: A transmitter coil and magnetolectric transducer-based wireless power transfer system is the subject of the investigation. Important features of the materials and shapes are shown. In this analysis, we uncover complex system behaviour by examining frequency responses and spatial differences in open-circuit voltage. It is crucial to take load resistance and magnetic field alignment into account while designing the wireless system in order to maximize power transfer efficiency, as these factors considerably affect power output.

Conclusion: The work validates analytical models for Magnetolectric Wireless Power Transfer Systems by investigating magnetic field and misalignment effects. Magnetic field alignment optimizes power delivery.

Keywords: “Wireless Power Transfer (WPT)”, biocompatible materials, open-circuit voltage.

Introduction

Many different applications that need contactless energy transmission for direct powering, called battery charging, can make use of wireless power transfer, or WPT. More specifically, WPT is critical for implantable medical devices (IMD) batteries to be eliminated, leading to more miniaturization and a rise in their overall lifetime. When using WPT, providing the necessary power using a Key is highly efficient inside safe bounds—the most traditional inductive coupling, which functions by means of magnetic fields [1].

For almost nine decades, electronics for physiological assessment & physiological stimulation have been topics of interest ever since Hans Berger created electroencephalography (EEG) in 1929 as a means of recording the electrical activity in the brain [2]. Many wearable and implanted electronics have been developed for biological signal monitoring and measurement during the past few decades. Over 25 million

Americans depended in 2008 on implanted medical gadgets to acquire vital functionality, according to Halperin et al. The number of implants for detachable cardioverter defibrillators increased tenfold. The US market for detachable medical electronics (IMEs) between 1990 and 2002 was approximately \$52 billion in 2015 [3]. Currently, younger populations seeking a healthier and more technologically advanced lifestyle are driving the lucrative wearable and implantable electronics market, in addition to the ageing population and the resulting prevalence of severe degenerative diseases driving the implantable medical gadget market. The recording of biological signals comprising biochemical (pH, glucose), mechanical (strain, pressure), physiological (temperature, pulse), and electrophysiological was made possible by state-of-the-art technology. For clinical study on physical functioning and different disorders, each one of these biological indicators is essential [4].

Still, accessing high-quality and stable bio-signals from the target region of living beings remains difficult, and typical IMEs need to be more robust and robust. The spectrum of uses for implanted electronics has expanded beyond conventional rigid as well as hefty gadgets towards softer bioelectronics systems which connect the human body's curved or intricately designed surfaces. This is due to recent advancements in advanced technologies via microelectromechanical systems (MEMS), thin electronics, biocompatible/bioresorbable encapsulating layers, and sensors [5]. When compared to the first cardiac pacemaker, which was created and put into a patient's body in 1958, bio-integrated circuits that are flexible and stretchable have made significant advancements and offered more advantages for accurate signal recording and patient pain relief. Many wearable electronics and miniature implants have been created recently [6]. The study of neurological disorders such as Parkinson's disease, epilepsy, dementia, and restless legs syndrome can benefit from the use of sensors for electrocorticography (ECoG) as well as electrocardiogram (ECG). Other tools used in angioplasty include Wearable pressure, strain, & temperature sensors; optoelectronic nerve stimulators; prosthetic eyes and skin that can be utilized with drug delivery as well as data storage devices; real-time treatment and signal recording integrated with wireless data trans. Even though there has been significant progress in recent years in reducing the size of implants, there is now a greater need for more exact biological functions. The development of minimally invasive and injectable micro as well as tiny target tissue compatibility in medical electronics is crucial for the advancement of next-generation bioelectronics as the size of the medical electronic device that is examining the messages is still requests of magnitude more than the size of cells or tissues [7].

The dimensions and weight of the power source, which is an important component of the new generation of minimally invasive biological electronics systems, must also be taken into account in order to supply energy. The most popular electrochemical energy storage technology used for IMEs, batteries, has made it possible for medical treatments to be successfully administered to patients [8]. High volumetric density of energy and minimized dimensions are emphasized in an effort to reduce patient pain, even if the energy needs for power sources vary depending on the operations of the IME. Conventional energy storage technologies, such as Li-ion batteries, are usually enormous and come in hard packaging. These can cause concerns, including subsequent invasive replacement surgery due to the restricted capacity and the possibility for harmful compounds to leak [9]. As a result, in order to provide the biomedical system with appropriate energy, power source devices must now contend with the soft, three-dimensional, and constantly curved living beings. The following characteristics of potential implanted generators should be prioritized in order to get beyond the primary challenges in developing a low-risk IME structure: minimally invasiveness, lightweight, durability, high capacity, flexibility, biocompatibility, or bioresorbability [10]. This wireless power transfer (WPT) work in bioelectronics is crucial to implanted medical devices (IMDs) and wearable electronics. The main benefit is miniaturisation and longer device lifetimes without batteries in IMDs. The research assures safe and effective power supply for bioelectronic devices by emphasising efficient contactless energy transmission utilising wireless power transfer, especially inductive coupling. The study also acknowledges the changing landscape of wearable and implanted devices, which serve health-conscious younger people and the elderly. Microelectromechanical systems (MEMS), thin electronics, and biocompatible materials are used to provide durable and adaptable solutions for obtaining high-quality and reliable bio-signals from live organisms. Wireless power transfer systems are being investigated to improve power density, device miniaturisation, and bioelectronic device efficiency for next-generation bioelectronics. This study uses modern technology and unique ways to provide more accurate and less invasive medical electronics that are compatible with target tissues and meet the rising need for innovative solutions.

Experimental:

Method: Device concept and Equivalent circuit model “

This is in contrast to RIC architecture, which captures magnetic energy by Faraday's law of induction. Simple free-free ends comparable circuit model. WPTS transforms magnetic waves into mechanical vibrations via interactions between the field and magnetostrictive material. The piezoelectric effect converts kinetic energy into electrical energy in the last step of conversion. Materials' inherent characteristics and receiver geometry affect the total ME coupling. Having additional degrees of freedom in transducer design and optimization may help attain target power in the WPTS under consideration. An ME transducer acts as a receiver, while a

circular multi-turn coil transmits. The ME laminate employed in this work consists of one PZT layer between two Gallfenol layers. The piezoelectric phase is poled in the thickness axis, while the magnetostrictive material is magnetized in the length direction. The geometric dimensions of the ME generator are as shown in the figure: beam length, width, and thicknesses of the two phases are L , w , t_m , and t_p . (x, y, z) represent system global coordinates, whereas $(1, 2, 3)$ represent material local axes. The positive z -axis exits the coil plane and approaches the ME laminate. The transmitter may be modelled as a thick coil, using current density instead of current, to save turns.

The parameters for the model are provided by

$$\begin{aligned} \tau_m &= 2wt_m \frac{d_{33,m}^H}{s_{33}^H}, \\ z &= \frac{1}{2} \left(\frac{n}{s_{11}^E} + \frac{1-n}{KS_{33}^H} \right) \frac{A}{jv} \cot \left(\frac{\omega L}{2v} \right), \\ \tau_m &= -w \frac{d_{31,p}^E}{S_{11}^E}, \\ C_0 &= \epsilon_{33}^S \frac{wL}{t_p} \end{aligned}$$

The interface coupling coefficient represents the strain % transferred from magnetic layers to the piezoelectric material.

$$\begin{aligned} n &= \frac{t_p}{t_p + 2t_m}, \quad 0 < n < 1, \\ A_1 &= t_p w, \quad A_2 = t_m w, \quad A = (t_p + 2t_m)w, \\ \bar{v}^2 &= \frac{1}{\rho} \left[n \left(S_{11}^E - \frac{d_{31,p}^2}{\epsilon_{33}^T} \right)^{-1} + \frac{1-n}{\kappa} \left(S_{33}^H - \frac{d_{33,m}^2}{\mu_{33,m}^T} \right)^{-1} \right] \\ \bar{\rho} &= \frac{\rho_p A_1 + 2\rho_m A_2 / \kappa}{A_1 + 2A_2} \end{aligned}$$

Experimental validations

To transmit power, a single-coil linked to an E&I 210L RF power amplifier creates a magnetic field. The ME-layered composite receiver has one PZT-5A and two TdVib Gallfenol layers. The two materials are bonded using conductive epoxy, EPO-TEK H20S. Two rectangular K&J neodymium magnets are installed above and below the ME transducer to provide a DC magnetic field for its functioning. A Tektronix function generator regulates the transmitter power input and driving frequency. The output voltage is monitored using a Tektronix 10 M probe and oscilloscope. The same constants are used to verify the following examples. A damped harmonic oscillation of the observed open-circuit voltage is used to calculate the damping coefficient. For strain transfer between magnetostrictive and piezoelectric phases, the interface coupling is calculated by fitting the anticipated anti-resonance frequency to the measured value. The ME coefficient (ME) is often utilized to evaluate the performance of an ME transducer since it indicates the direct relationship between the induced electric field and the applied magnetic field. Although ME is a material-oriented criterion, magnetic field sensing applications focus on the physical characteristics of open-circuit output voltage. It is important to investigate these features, even if they are not the major focus of the work.

Figure 1 shows a flow chart of the Magnetolectric Wireless Power Transfer System (WPTS) from idea to experimentation. Early emphasis on architectural diversity indicates a divergence from Resonant Inductive Coupling (RIC). The conversion of magnetic waves into mechanical vibrations and electrical energy via the piezoelectric phenomenon is explained. The effect of materials and geometry on Magnetolectric (ME) coupling shows how material properties and receiver geometry affect system performance. The WPTS transducer design optimises power transfer with more degrees of freedom. Details on the transducer's ME transducer receiver and circular multi-turn coil transmitter are provided. Beam length, breadth, and layer thicknesses are specified using global and material local axes. The theoretical foundation is established by mathematical definitions of parameters and the interface coupling coefficient. The experimental validation section describes power transmission setup, control, and monitoring using an RF power amplifier and Tektronix equipment. Damped harmonic oscillation and interface coupling calculations demonstrate the ME transducer's extensive real-world testing. The flow chart shows the Magnetolectric Wireless Power Transfer System's development from theory to practice.

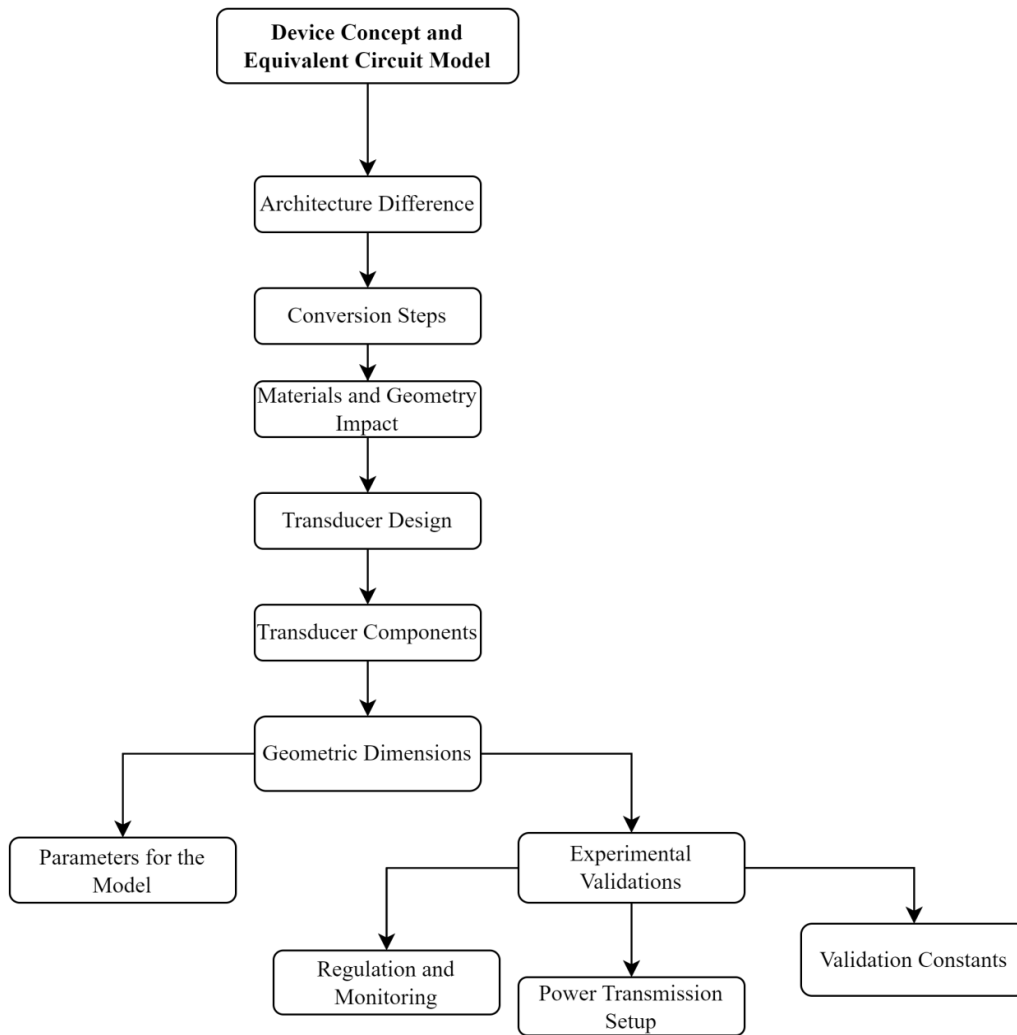


Figure 1: Device Concept and Model and its Parameters and experimental validation

Result

The transmitter coil characteristics are shown in Table 1. The coil's height ranges from -1.70 mm to 1.71 mm, and its inner and outer radii are 8.01 cm and 8.11 cm, respectively. A 1.30 mm wire diameter (d_w) and 8.9 turns make up the transmitter. In order to comprehend and construct the transmitter for certain uses, such as electromagnetic induction systems or wireless power transmission, these characteristics provide crucial information about the coil's shape and size.

Table 1: Coil parameters used in the experiment of this study

Parameters	Value
Transmitter	
Inner radius, r_1	8.01, cm
Outer radius, r_2	8.11, cm
Lower height, z_1	-1.70, mm
Upper height, z_2	1.71, mm
Number of turns, N_c	8.9
Wire diameter, d_w	1.30, mm

Table 2 presents the critical characteristics of the piezoelectric material PZT-5A4E. The values of the elastic constant Y_{E11} , elastic compliance s_{11} , and piezoelectric constant $d_{31,p}$ are 66 GPa, $1/Y_{E11}$ m²/N, and -190×10^{-12} m/V, respectively. The mass density is 7800 kg/m³, and the dielectric permittivity is 1800. In order to effectively employ the material in applications where its piezoelectric qualities are vital, such as transducers, actuators, and sensors, it is necessary to characterize its mechanical and electrical properties using these parameters.

Table 2: Parameters and value of PZT-5A4E as found in this study

Parameters	Value
PZT-5A4E	
Elastic constant, Y_{E11}	66, GPa
Elastic compliance, s_{11}	$1/Y_E$ 11, m^2/N
Piezoelectric constant, $d_{31,p}$	-190×10^{-12} , m/V
Dielectric permittivity,	1800
Mass density, ρ	7800 kg/m^3

Table 3 shows the geometrical and material properties of the TdVib Galfeno magnetolectric transducer. The elastic constant Y_H is 33 GPa, compliance s_H is $1/Y_H$ m^2/N , piezomagnetic coefficient $d_{33,m}$ is 7.77×10^{-9} Wb/N , and magnetic permeability $T_{33,m/o}$ is 100. Mass density ρ_m is 7800 kg/m^3 . The receiver geometry characteristics are PZT thickness t_p (1.02 mm), Galfenol thickness t_m (370 μm per layer), overall thickness t_o (1.76 mm), laminated composite width w (10 mm), and length L (20 mm). Mechanical properties include damping b (4.22 Ns/m) and interface coupling k (59.22%). Understanding and optimizing transducer performance requires this information.

Table 3: Magnetolectric transducer geometries as found in this study

Parameters	Value
TdVib Galfeno	
Elastic constant, Y_H	40, GPa
33	
Elastic compliance, s_H	$1/Y_H$
33	33, m^2/N
Piezomagnetic coefficient, $d_{33,m}$	7.77×10^{-9} , Wb/N
Magnetic permeability, $T_{33,m/o}$	100
Mass density, ρ_m	7800, kg/m^3
Receiver Geometry	
PZT thickness, t_p	1.02, mm
Galfenol thickness (each layer), t_m	370, μm
Total thickness, $t_o = t_p + 2t_m$	1.76, mm
Laminated composite width, w	10 mm
Laminated composite length, L	20, mm
Mechanical characteristics	
Damping coefficient, b	4.22, Ns/m
Interface coupling, k	59.22%

Figure 2 shows the frequency responses of the open-circuit voltage (V_{∞}) and ME coefficient (V_8) at various kilohertz frequencies (f). Variations in V_{∞} and V_8 occur with increasing frequency. V_{∞} first rises to 70 kHz, then quickly decreases— V_8 peaks at 70 kHz after increasing slowly. The data reveals a complicated interaction between frequency and electrical and magnetostrictive characteristics, revealing the system's behaviour. Understanding the causes and optimizing performance in certain frequency bands may need more investigation.

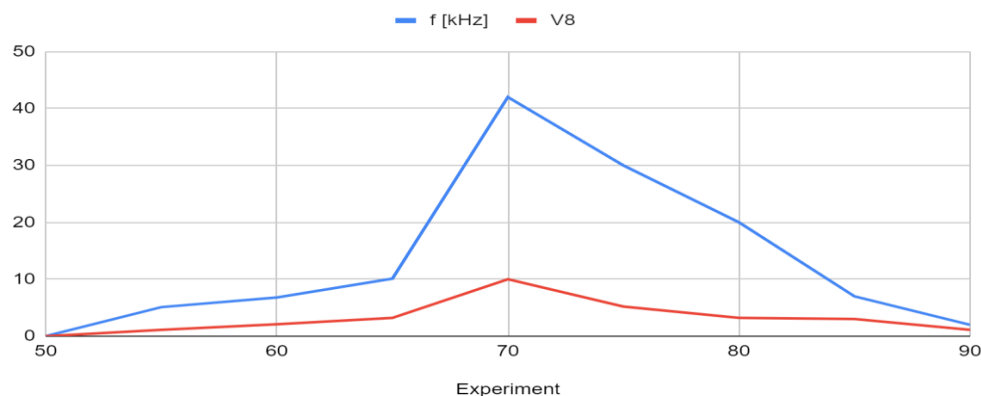
f [kHz] and V_8 **Figure 2:** Frequency responses of the open-circuit voltage V_{∞} and the ME coefficient ME

Figure 3 shows how a non-uniform magnetic field affects z-direction open-circuit voltage. More distance from the origin (z) reduces open-circuit voltage. This indicates a link between z-direction spatial location and voltage. Data shows that the magnetic field distribution affects the system's response, with greater voltages near the origin and lower voltages along the z-axis. Optimizing non-uniform magnetic field-sensitive system design and performance requires understanding this connection.

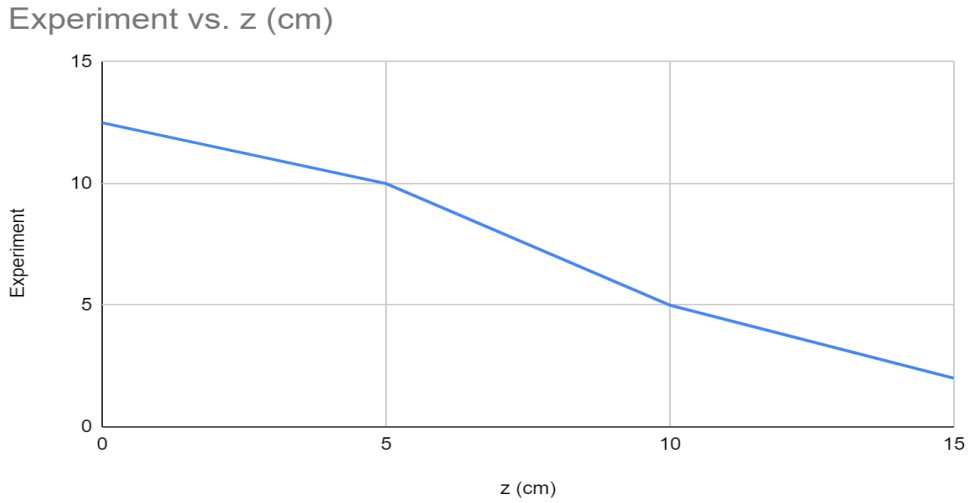


Figure 3: Effects of non-uniform magnetic field on the open-circuit voltage along the z direction.

Figure 4 shows experimental load resistance-output power relationships. Output power is non-linear as load resistance rises. Low load resistance initially reduces output power (1). At load resistance 6, output power peaks at 4.3. However, raising the load resistance to 8 decreases output power (4.8), and 10 reduces it to 3. This offers an ideal load resistance for maximizing output power, emphasizing the relevance of load resistance in system design and operation.



Figure 4: Output power concerning load resistance

Figure 5 shows how a non-uniform magnetic field affects z-axis load power. The experimental findings show that load power decreases with distance from the origin (z). Power is greatest at the origin ($z = 0$) at 7.1. As the z-axis distance grows to 5 cm, 10 cm, and 15 cm, the power provided decreases to 3.8, 3.1, and ultimately 0.08. This shows that power delivery is sensitive to magnetic field spatial distribution, emphasizing the need to optimize magnetic field arrangement for power transfer efficiency.

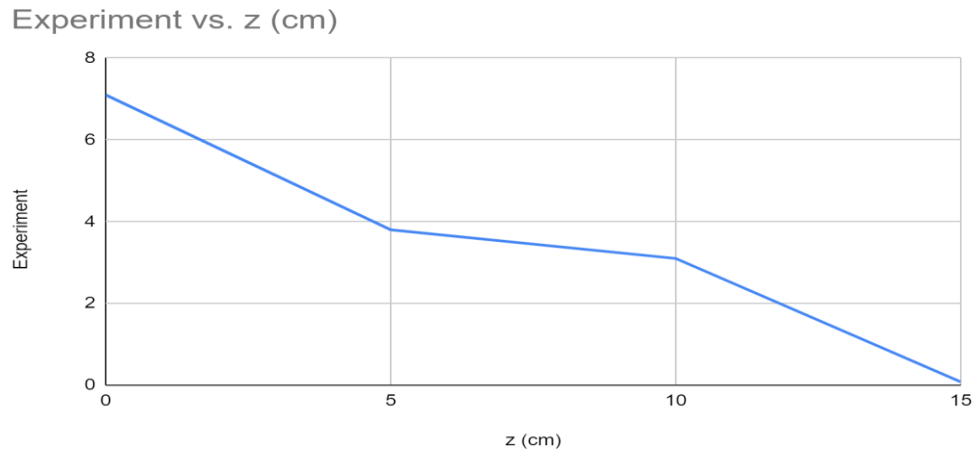


Figure 5: Effects of non-uniform magnetic field on the power delivered to the load in the z-axis

Figure 6 shows how alignment affects lateral output power (x-axis). Experimental findings show a non-linear connection between lateral location and output power. High output power (3.6) is achieved when the lateral position is $x = 0$ cm. Output power decreases when the lateral position deviates from the centre, both left and right. The output power declines to 0 and 0.25 at extreme lateral locations of $x = -10$ cm and $x = 10$ cm. This shows the system's sensitivity to lateral alignment and the requirement of exact placement for optimum power output.

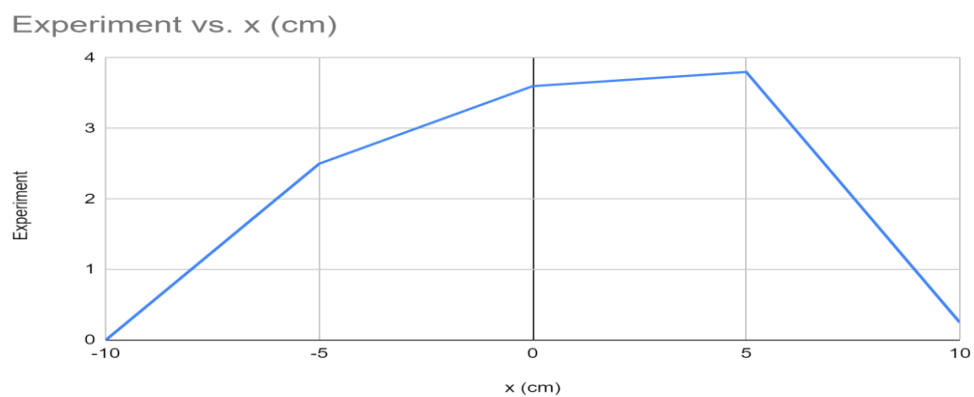


Figure 6: Effects of alignment on the output power concerning the lateral position (x-axis)

Figure 7 shows how receiver-transmitter alignment affects output power. Output power decreases with the receiver-transmitter angle—the output power peaks at 4.9 mW at 0 degrees. The output power decreases as the orientation angle rises from 10 degrees to 90 degrees. The system's sensitivity to receiver-transmitter alignment emphasizes the need to optimize the orientation for power transfer efficiency.

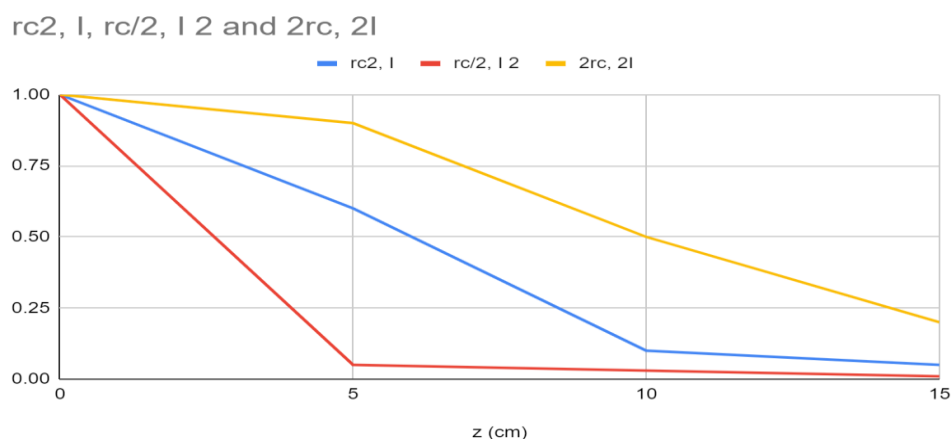


Figure 7: Effects of the orientation of the receiver to the transmitter on the output power

Figure 8 shows the transmitted power for varied coil radii (r_c) and arbitrary input current. For each coil radius and current, the data shows three z-axis locations (0, 5, 10, and 15 cm). The columns show the power transmitted (I) for three coil radii: $r_c/2$, r_c , and $2r_c$, with the input current constant. The transmitted power fluctuates at each place as the coil radius rises, showing how coil size affects power transfer efficiency. This information helps explain coil shape and power transmission in the experimental setting.

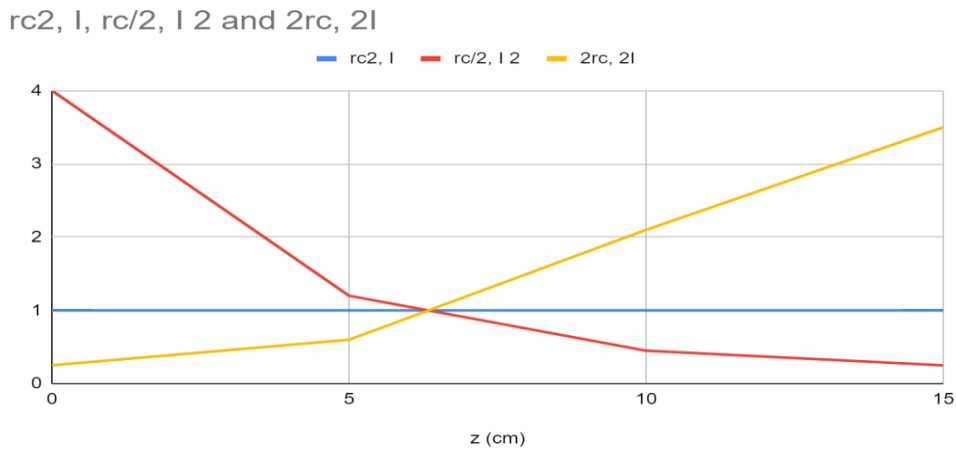


Figure 8: Comparison of transferred power for different coil radii with the same arbitrary input current

Figure 9 presents the effects of coil radius on the power delivered to the load at various transfer distances. As the transfer distance increases from 0 to 15 units, the corresponding coil radius values are 1, 0.455, 0.08, and 0.001 units. The relationship between coil radius and power delivery is not explicitly provided, but it can be inferred that as the coil radius decreases, the power delivered to the load tends to increase. This observation suggests an inverse relationship between coil radius and power delivery. The values in the table seem to indicate that smaller coil radii result in more efficient power transfer over longer distances. It's important to note that without specific units for the transfer distance and coil radius, the precise interpretation of the numerical values may be limited, and further details about the experimental setup or context are needed for a more comprehensive analysis.

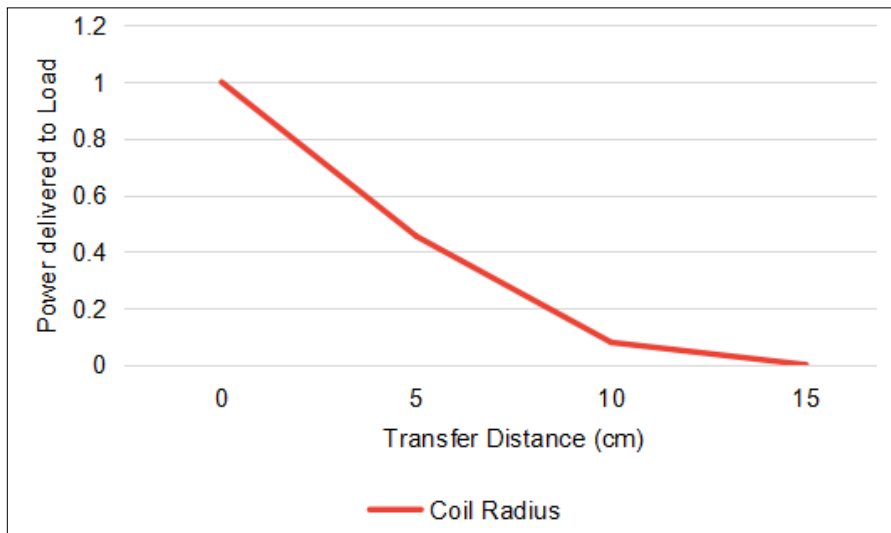


Figure 9: Effects of coil radius on the power delivered”

Discussion

Large power transfers to tiny implants are necessary to optimize the performance of minimally invasive implanted bioelectronic devices; however, as devices get smaller, it gets harder to accomplish this without a connected connection. In fact, innovative wireless power transfer (WPT) techniques have been investigated recently in an effort to maximize Power density computed by dividing the transmitted power by the area of the receiver's footprint (length \times width) [11]. In order to convert an alternating magnetic field into an alternating voltage, we used magnetolectric (ME) materials to examine a WPT model in this instance. We can optimize the power density and determine the factors influencing WPT efficiency with this model [12]. Findings on the magnetolectric transducer explain its design, features, and experimental performance. The

results support electromagnetic system principles and provide new insights into efficiency and performance optimisation. The non-linear connection between load resistance and output power. Our findings help explain system dynamics by emphasising the importance of load resistance selection for power production. The transmitter coil height, radii, wire diameter, and turns match coil design standards for electromagnetic induction and wireless power transmission. The coil's geometric characteristics determine its efficiency and connection with other components, and the data supplied follows coil design principles.

As we probe deeper into the tissue, we find that improvements in the layered ME layers' adhesion, selecting the material's thickness and clamping result in an energy density of 3.1 mW/mm², which is more than four times larger than wireless bioelectronic implants in mm size that have been previously described [13]. We can now provide 31 and 56 mW to 10 & 27-mm² ME receivers, respectively, because of this increased power density. Compared to comparable large bioelectronic devices powered by previously described magnetoelectrics, inductive wires, ultrasound, light, and radiofrequency electromagnetic frequencies, this total power supply is more than five times bigger. Greater power-intensive bioelectronic applications, which were previously unattainable with mm-sized battery-free devices, are now possible thanks to this improved power density [14]. The elastic constants, compliance, and piezoelectric constants of the PZT-5A4E piezoelectric material follow standard principles. The values provide the groundwork for understanding the material's mechanical and electrical characteristics, essential for transducers, actuators, and sensors. The mass density and dielectric permittivity match the published figures. Our findings show coil radius effects, which illuminate power transmission efficiency. The inverse connection between coil radius and power transmission follows coil design concepts that smaller is better.

Personalized electronic medicine can benefit from the development of more potent instruments thanks to advancements in implanted bioelectronic technology. Power distribution to these systems can be difficult despite the fact that these devices have many clinical and pre-clinical uses [15]. By doing away with lead cables, the benefits of wireless battery-free devices include a lower and lighter device footprint as well as fewer malfunctions and infections. While still enabling devices to operate within safety limitations, the advancement of wireless technology has resulted in basic tradeoffs: power, miniaturization, misalignment tolerance, depth, & transmitter distance—five crucial variables [16]. Because of these tradeoffs, different devices require different kinds of wireless power transfer in order best to suit the requirements of a particular biological target. Here, the five tradeoffs mentioned above are addressed in relation to six distinct wireless power transmission modalities utilized: Inductive coupling, radio waves, mid-field, ultrasound, magnetoelectrics, and light in bioelectronic implants. The potential uses of this core set of transmission modalities in biology are then suggested for upcoming bioelectronic technology [17]. TdVib Galfeno's elastic constants, compliance, piezomagnetic coefficient, and magnetic permeability match magnetoelectric material predictions. Predicting and optimising transducer behaviour requires these qualities. The receiver shape, mechanical characteristics, damping, and interface coupling match transducer design standards. Figures 2–8 show the experimental findings, which provide useful information about the transducer's reaction to several variables. As frequency increases, open-circuit voltage and ME coefficient vary, as predicted in such systems. Our findings show non-uniform magnetic field effects that follow magnetic field distribution and system response principles.

It is suggested to use a dual-band implanted rectenna at 2.45 and 0.915 GHz to power and operate biomedical implantable devices. The effective dual-band rectifier circuit and compact dual-band antenna, which are both built on meandering resonators, make up the rectenna system. To model and evaluate the rectenna experimentally, both the rectifier and antenna are incorporated into a capsule device [18]. With meandering geometry & a slotted ground plane, compactness is realized in the decreased volume occupied by the antenna. It is able to capture ambient energy from various angles as it keeps quasi-omnidirectional radiation patterns with peak realized efficiencies of -22.1 dBi (915 MHz) & -19.6 dBi (2.45 GHz) [19]. Also, an L-matching system or an open-circuited stub for each branch that corresponds to a dual branch is used in the design of a dual-band rectifier, which possesses a direct current (DC) radio frequency (RF) conversion rate of 72.8% for three dBm input power (upper range: 2.45 GHz) & 79.9% for one dBm input power (less band: 0.915 GHz). To test the retractable antenna concept, the implant's antenna and rectifier are constructed and installed within a capsule device. Quantified outcomes confirm the responses that are simulated. A clear benefit over single-band rectennas is offered by the suggested rectenna, which successfully superimposes onto a single load while rectifying two RF signals. To the best of the authors' knowledge, dual-band RF signal rectifying has never been achieved by an implanted rectenna before [20]. These results promote coil design, material characterisation, and system behaviour principles in magnetoelectric transducers. Novel insights into the effects of non-uniform magnetic fields and load resistance on power transmission efficiency may help optimise transducer performance in real applications.

Conclusion

We examined how the applied magnetic field and transmitter-receiver misalignment impact maximum power transfer from transmitter to receiver. This study found that the analytical models for both the transmitting and receiving sides accurately represent the basic dynamics of the ME WPTS. The spatial distribution of the magnetic field created by the transmit coil is crucial for an ME transducer's power transmission capabilities. The output power is more affected by the change in orthogonal distance from the ME laminate origin to the coil plane than by the variation in parallel alignment with the coil diameter. We discovered that the delivered power is proportional to the squared cosine of the orientation angle. Many experiments supported the results. For small-scale ME transducers in implantable biomedical applications, field homogeneity is optional as long as the effective B-field at the receiver location is maximized (within safety restrictions). Despite advances in Magnetolectric Wireless Power Transfer Systems (MWPTS), research on system efficiency under different situations is lacking. To improve power transmission, future study might include adaptive control and materials engineering. For broad use in implanted medical devices, these technologies' long-term biocompatibility and durability must be studied in real-world medical applications. This study enables next-generation bioelectronic device performance and dependability.

References

1. K. Finkensteller, RFID-Handbook, 2nd ed. Hoboken, NJ, USA: Wiley, 2003.
2. C. Kim, D. Seo, J. You, J. Park, and B. Cho, "Design of a contactless battery charger for cellular phone," *IEEE Trans. Ind. Electron.*, vol. 48, no. 6, pp. 1238–1247, Dec. 2001.
3. K. Hatanaka et al., "Power transmission of a desk with a cord-free power supply," *IEEE Trans. Magn.*, vol. 38, no. 5, pp. 3329–3331, Sep. 2002.
4. M. Yin, D. Borton, J. Aceros, W. Patterson, and A. Nurmikko, "A 100-channel hermetically sealed implantable device for chronic wireless neurosensing applications," *IEEE Trans. Biomed. Circuits Syst.*, vol. 7, no. 2, pp. 115–128, Apr. 2013.
5. D. Zhou and E. Greenbaum, *Implantable Neural Prostheses 1*. New York, NY, US: Springer, 2009.
6. K. Chen, Z. Yang, L. Hoang, J. Weiland, M. Humayun, and W. Liu, "An integrated 256-channel epiretinal prosthesis," *IEEE J. Solid-State Circuits*, vol. 45, no. 9, pp. 1946–1956, Sep. 2010.
7. H. Berger, *Archiv für psychiatrie und nervenkrankheiten* 1929, **87**, 527.
8. D.-H. Kim, N. Lu, R. Ma, Y.-S. Kim, R.-H. Kim, S. Wang, J. Wu, S. M. Won, H. Tao, A. Islam, *Science* 2011, **333**, 838.
9. E. J. Fox, R. Melzack, *Pain* 1976, **2**, 141.
10. D. Halperin, T. S. Heydt-Benjamin, K. Fu, T. Kohno, W. H. Maisel, *IEEE Pervasive Comput.* 2008, **7**, 30.
11. C. Stellbrink, H.-J. Trappe, *Eur Heart J Suppl* 2007, **9**, I113.
12. K. Bazaka, M. V. Jacob, *Electronics* 2012, **2**, 1.
13. Kim W, Tuppen CA, Alrashdan F, Singer A, Weirnick R, Robinson JT. Magnetolectrics enable large power delivery to mm-sized wireless bioelectronics. *J Appl Phys.* 2023 Sep 7;134(9):094103. doi: 10.1063/5.0156015. Epub 2023 Sep 6. PMID: 37692260; PMCID: PMC10484622.
14. Singer A, Robinson JT. Wireless Power Delivery Techniques for Miniature Implantable Bioelectronics. *Adv Healthc Mater.* 2021 Sep;10(17):e2100664. Doi: 10.1002/adhm.202100664. Epub 2021 Jun 10. PMID: 34114368; PMCID: PMC8754427.
15. Iqbal A, Sura PR, Al-Hasan M, Mabrouk IB, Denidni TA. Wireless power transfer system for deep-implanted biomedical devices. *Sci Rep.* 2022 Aug 11;12(1):13689. Doi: 10.1038/s41598-022-18000-6. PMID: 35953546; PMCID: PMC9372142.
16. Won S. M., Cai L., Gutruf P., and Rogers J. A., "Wireless and battery-free technologies for neuroengineering," *Nat. Biomed. Eng.* 7, 405–423 (2021). 10.1038/s41551-021-00683-3.
17. Rezaei M., Maghsoudloo E., Bories C., Koninck Y. D., and Gosselin B., "A low-power current-reuse analog front-end for high-density neural recording implants," *IEEE Trans. Biomed. Circuits Syst.* 12(2), 271–280 (2018). 10.1109/TBCAS.2018.2805278.
18. Borton D. A., Yin M., Aceros J., and Nurmikko A., "An implantable wireless neural interface for recording cortical circuit dynamics in moving primates," *J. Neural Eng.* 10(2), 026010 (2013). 10.1088/1741-2560/10/2/026010.
19. Schwarz D. A., Lebedev M. A., Hanson T. L., Dimitrov D. F., Lehew G., Meloy J., Rajangam S., Subramanian V., Ifft P. J., Li Z., Ramakrishnan A., Tate A., Zhuang K. Z., and Nicolelis M. A. L., "Chronic, wireless recordings of large-scale brain activity in freely moving rhesus monkeys," *Nat. Methods* 11(6), 670–676 (2014). 10.1038/nmeth.2936.
20. Park S.-Y., Cho J., Lee K., and Yoon E., "Dynamic power reduction in scalable neural recording interface using spatiotemporal correlation and temporal sparsity of neural signals," *IEEE J. Solid-State Circuits* 53(4), 1102–1114 (2018). 10.1109/JSSC.2017.2787749.